Letters

Active Metallic Photonic Band-Gap Materials (MPBG): Experimental Results on Beam Shaper

G. Poilasne, P. Pouliguen, K. Mahdjoubi, L. Desclos, and C. Terret

***Abstract*—We focus our attention on the possibilities to control the beam radiated by antennas, which are initially omnidirectional using active metallic photonic band-gap materials (AMPBG). In fact, MPBG composed of continuous or discontinuous wires present different and interesting characteristics when they are used as antenna reflector or radome. Adding active components on wires allows to switch from continuous to discontinuous structures. Wires with active elements on can then be placed inside a structure, which shapes the beam radiated by a dipole antenna. Experimental results show that it allows to switch on/off the beam or to change its shape.**

***Index Terms*—FET, metallic photonic band-gap materials (MPBG), radiation patterns.**

I. Introduction

Metallic photonic band-gap materials (MPBG) are periodic structures composed of metallic parts [1]. They exhibit frequency bands for which no propagation mode is allowed [2]. MPBG composed of continuous or discontinuous wires have different behaviors, which we recall in Section II. To switch from continuous to discontinuous wires, active components are added to the wires. The structures are studied using a moment method with passive elements to model active device states. It shows that just few switchable wires are enough to either turn on/off or to shape in different ways, the beam radiated by a dipole antenna placed inside an active MPBG. These theoretical results are presented in Section III and then validated experimentally in Section IV.

II. Comparison Between Continuous and Discontinuous MPBG

Continuous wire MPBG [two-dimensional (2-D) lattices] and discontinuous ones [three-dimensional (3-D) lattices] have completely different behaviors even if they have the same period and the same wire diameter Fig. 1(a). In fact, for continuous wire MPBG excited by a plane wave with the *E*-field parallel to the wire axis, the reflection coefficient is equal to 1 from 0 Hz to a cutoff frequency, which depends on the physical parameters. This first band gap is followed by a propagation band. Propagation peaks within this band correspond to directive modes of the structure, which can help, for example, to reduce grating lobes [3]. In the case of discontinuous wire MPBG, the transmission coefficient looks like that of all dielectric PBG [4], which are band reflectors. The response of discontinuous wire MPBG depends on the classical 2-D MPBG parameters, i.e., the period in both directions and the wire diameter. This response depends also on the wire length. An optimal length can be found in order to obtain the band gap presenting the largest bandwidth. This duality between continuous and discontinuous MPBG is all the more important as a frequency can be within a band gap for one of the structures and within a propagation band of its dual. This is the reason why we are interested in active structures, which can allow to switch from one case to the other one.

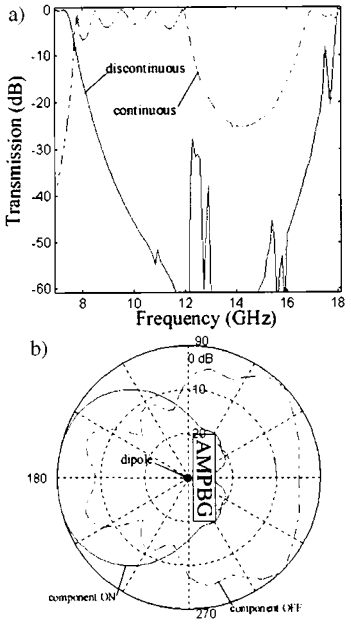

Fig. 1. (a) Transmission coefficient of two MPBG (12-mm period, 2-mm wire diameter): one composed of continuous wires and the other composed of discontinuous ones. (b) Radiation patterns of a dipole antenna placed above an active MPBG, for both states of the components: ON (equivalent to continuous structure) and OFF (equivalent to discontinuous one).

An active MPBG (AMPBG) is composed of discontinuous wires on which are placed active components. To simulate active wires, we use a moment method [5]. As field effect transistors have simple equivalent model in ON–OFF states, we implement these models on the corresponding segments in the simulation. Fig. 1(b) shows the radiation patterns obtained when a dipole antenna, placed above an active (A)MPBG, is excited at a frequency within the band gap of the continuous wire MPBG and within the propagation band of the discontinuous one. The patterns show that the structure behaves like a reflector when the active components are ON (equivalent to a short circuit), or just like a scatterer when they are OFF (equivalent to an open circuit).

III. Potential Use of Active MPBG

When a dipole is placed inside a MPBG, either its frequency corresponds to a band gap and the far field is low or the frequency is within a propagation band and the radiation pattern has beams in the propagation mode directions. In the first case, where the excitation is within a band gap, a row of wires can be suppressed in order to create a guiding structure. The field propagates within the structure and the radiation pattern is the same as the one obtained with an open guide [6]. Here, we replace some of the continuous wires by active ones Fig. 2(a).

Manuscript received April 28, 1999; revised October 11, 1999.

G. Poilasne was with LSR/Laboratoire Antennes et Télécommunications, UPRES-A CNRS 6075, Université de Rennes I, Campus de Beaulieu, 35042 Rennes Cedex, France. He is now with the Electrical Engineering Department, University of California, Los Angeles, CA 90095-1594 USA.

P. Pouliguen, K. Mahdjoubi, and C. Terret are with LSR/Laboratoire Antennes et Télécommunications, UPRES-A CNRS 6075, Université de Rennes I, Campus de Beaulieu, 35042 Rennes Cedex, France.

L. Desclos is with NEC Corporation, C&C Media Laboratory, Network Laboratories, Miyamae-ku Kawasaki, Kanagawa, 216 Japan.

Publisher Item Identifier S 0018-926X(00)01284-9.

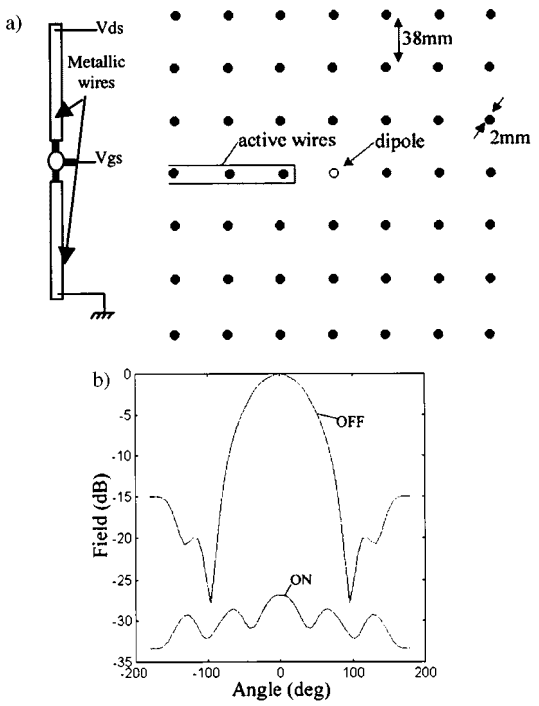

Fig. 2. Active wires inserted inside a 2-D MPBG composed of continuous wires with a dipole antenna placed in the middle. (a) Active wire and active structure geometry. (b) Numerical radiation patterns obtained for both component states at a frequency within the band gap of the continuous structure.

Different possibilities can be considered. The dipole can be excited at a frequency within the band gap of the continuous wire structure Fig. 2(b). Therefore, when the components are OFF, the row of active wires is equivalent to a row of discontinuous ones, the field propagates along this row and a wide beam is radiated. When the components are ON, the structure is like a completely continuous one, the beam is turned off. Active wires can be inserted in the four orthogonal directions to scan in all around as the 3-dB beam width is about $\pm 45^{\circ}$.

At the frequency corresponding to the first propagation peak of the continuous structure, the radiation pattern has narrow beams radiated in the four orthogonal directions, when the structure is symmetric. This radiation pattern is presented in Fig. 3 when the components are ON. When they are switched OFF, the structure has discontinuous wires in the corresponding direction. As the propagation is more fluid for discontinuous structures than for the first propagation mode of continuous ones, the pattern presents a wide beam in that direction, as presented in Fig. 3 as well.

IV. Experimental Validation

In order to validate the behaviors presented in Section III, active wires have been mounted in a MPBG. A structure already characterized experimentally has been used. It is a six-layer and 38-mm period MPBG with metallic wires of 2-mm diameter. With only six layers, just two active wires have been inserted. These wires are composed of two parts joined with a field-effect transistor Fig. 2(a). In order to reduce the leakage of microwaves in the feeding system inductances are added. Radiation patterns have been measured between 2.0–2.4 GHz using a printed dipole fed by a Lecher line already presented. As the end of the first band gap is at 2.2 GHz, this band is enough to analyze the system and to exhibit the phenomenon.

Excited at 2.1 GHz, the beam can be turned ON or OFF depending on the component state Fig. 4(a). The field radiated on the main axis can be

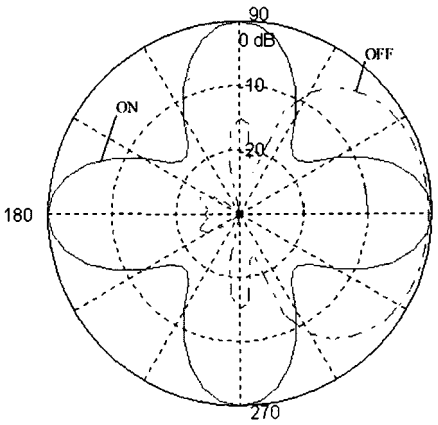

Fig. 3. Numerical radiation patterns obtained for both component states at the frequency corresponding to the first propagation peak of the continuous structure.

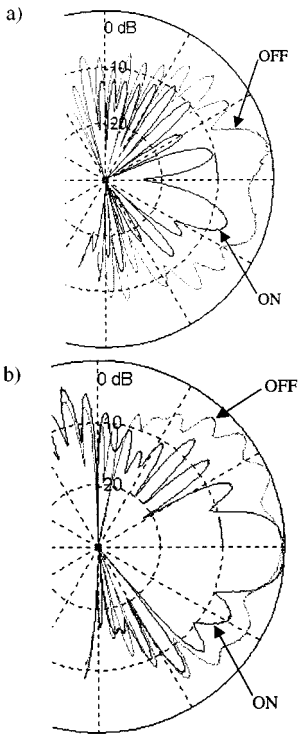

Fig. 4. Active wires inserted inside a 2-D MPBG composed of continuous wires with a dipole antenna placed in the middle. (a) Experimental radiation patterns obtained for both component states at a frequency within the band gap of the continuous structure (2.1 GHz). (b) Experimental radiation patterns obtained for both component states at the frequency corresponding to the first propagation peak of the continuous structure (2.3 GHz).

reduced of more than 15 dB. But in directions corresponding to $\pm 25^{\circ}$, the radiated field is not so much influenced by the active wire state. This is due to the fact that there are only two active wires. This structure also allows us to obtain the second behavior presented before. When the antenna is excited at 2.3 GHz, which corresponds to the frequency of the first propagation mode, we have been able to switch from a narrow beam to a wide one Fig. 4(b). In the ON state, the radiation pattern has a $\pm 15^{\circ}$ beamwidth whereas in the OFF one, the beam width is about $\pm 50^{\circ}$. We must also point out that the input impedance of the dipole used for experimentations and presented in [6] remains the same and is matched to 50 Ω for both component states.

V. Conclusion

We have presented the use of active device in MPBG beam control. Two behaviors have mainly been presented. The beam radiated by an antenna placed inside an AMPBG can be either turned ON or OFF or switched from a wide to a narrow one. An AMPBG has been realized and the radiation pattern has been measured for different frequencies validating the concept. Applications of such structures are now investigated.

References

[1] D. F. Sievenpiper, M. E. Sickmiller , and E. Yablonovitch, "3-D wire mesh photonic crystals," *Phys. Rev. Lett.*, vol. 76, no. 14, pp. 2480–2483, 1996.

[2] C. M. Soukoulis, *Photonic Band-Gap Materials*, ser. NATO ASI Ser., 1995.

[3] G. Poilasne, K. Madjoubi, P. Pouliguen, P. Gelin, and C. Terret, "Theoretical study of grating lobe reduction using metallic photonic band-gap materials," *Microwave Opt. Technol. Lett.*, vol. 18, no. 1, pp. 32–41, 1998.

[4] J. D. Joannopoulos, R. D. Meade, and J. N. Winn, *Photonic Crystals, Molding the Flow of Light*. Princeton, NJ: Princeton Univ. Press, 1995.

[5] G. Burke and A. Poggio, "Numerical Electromagnetics Code (NEC)," developed at Lawrence Livermore Lab., Livermore, CA, double precision version (nec2d).

[6] G. Poilasne, P. Pouliguen, K. Mahdjoubi, C. Terret, P. Gelin, and L. Desclos, "Radiation characteristics of and half wavelength dipole inside metallic photonic band gap structure," in *Proc. Antennas Propagat. Soc.*, Atlanta, GA, June 1998.

An Experimental Technique Used to Measure the Unloaded Q of Microstrip Antennas

Steven J. Weiss and Walter K. Kahn

***Abstract*—This paper presents a scattering method for measuring the unloaded Q of a prototype microstrip (patch) antenna structure without the need to implement connecting circuitry.**

***Index Terms*—Microstrip antenna, Q measurement.**

I. Introduction

An antenna illuminated by an electromagnetic wave will produce a scattered field. Quite generally this scattered field may be decomposed into two component parts: a component proportional to the field normally radiated when the antenna is excited by a voltage source and a component scattered by the antenna when the voltage source is short circuited [1]–[3]. This paper uses that concept in developing a measurement scheme that allows the unloaded Q of a prototype patch, modeled as a single RLC resonant circuit, to be determined *without the need to complete fabrication of the antenna with a connecting feed structure.*

II. Measurement Scheme

The prototype patch is placed on a large reflecting ground plane as depicted in Fig. 1. Two auxiliary antennas are used. Antenna #1 acts as transmitter, illuminating the patch with a main beam incident at an angle of approximately 45° to the ground plane (the x–y plane.) Antenna #2 acts as receiver and is placed directly above the patch with axis coincident with the z-axis. This orientation positions the receiving antenna outside the specular beam reflected from the ground plane. The polarizations of both auxiliary antennas are aligned in accordance with the desired radiation field of the patch antenna. Ideally, such an arrangement would be assembled in an electromagnetic anechoic chamber.

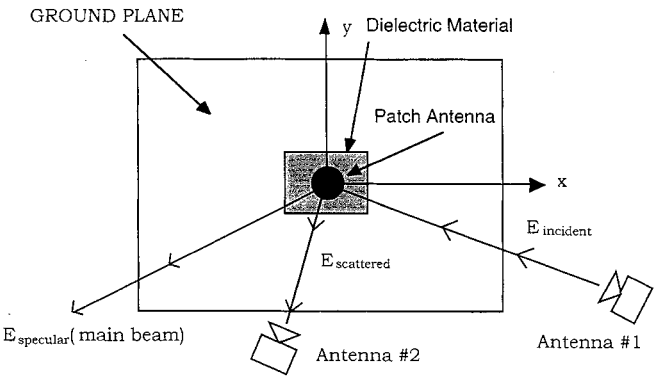

Fig. 1. Measuring the unloaded Q of a patch antenna.

Although the major portion of the incident field remains in a main beam specularly reflected from the ground plane E_{specular} (main beam), some is scattered in the z direction towards the auxiliary antenna #2 $E_{\text{scattered}}$ and detected. As indicated in the introduction, this scattered field comprises two components. One component of $E_{\text{scattered}}$ is a further composite: the reflected sidelobe of the auxiliary antenna #1, diffraction from the edges of the ground plane, and spurious contributions (reflections) from the surroundings. A second component of $E_{\text{scattered}}$ is due to the patch, which, excited as a resonator by the incident field, reradiates in just the same way as it would radiate when excited using a feed. This reradiated field carries the essential information related to the Q of the patch.

Our experiments were conducted in the 1–3 GHz region. The size of the large ground plane was 3 × 4 ft, and the auxiliary antennas were placed approximately 6 ft from the center of the plane. The largest linear dimension of the patches were on the order of 2 in. It follows that the auxiliary antennas were located in the near field of the reflecting ground plane and in the far-radiation field of the patch antenna. This will be seen to have a significant consequence in determining the relative phase relation between these two components of the scattered field.

III. Analysis and Results

An analysis of the scattering from a patch antenna structure, such as shown at the top of Fig. 2, is schematized in the remainder of that figure. The incident field and the total consequent scattered field are illustrated in Fig. 2(a) in two different ways: physically on the left and via a simplified equivalent circuit on the right. For instance, the incident field indicated on the physical picture is represented by the [Thevenin] generator E_α in the equivalent circuit. The radiation resistance of the patch antenna is shown as R_a; any reactance may be considered lumped with the impedance modeling the patch resonator Z_{resn}.

The current I_a in the circuit of Fig. 2(a), conventionally directed as shown, is easily found. The resonator impedance is then replaced by an equivalent ideal voltage generator $E_r = -I_a Z_{\text{resn}}$ in accordance with the circuit compensation theorem [2]. The principle of superposition then yields the two circuits shown in Fig. 2(b) and (c). For example, the current I_a is readily seen to be the algebraic sum of the currents in

Manuscript received May 30, 1996; revised July 1, 1999.

S. J. Weiss is with the U.S. Army Research Laboratory, AMSRL-SE-RM, Adelphi, MD 20783 USA.

W. K. Kahn is with the Department of Electrical and Computer Engineering, School of Engineering and Applied Science, George Washington University, Washington, DC 20052 USA.

Publisher Item Identifier S 0018-926X(00)01283-7.

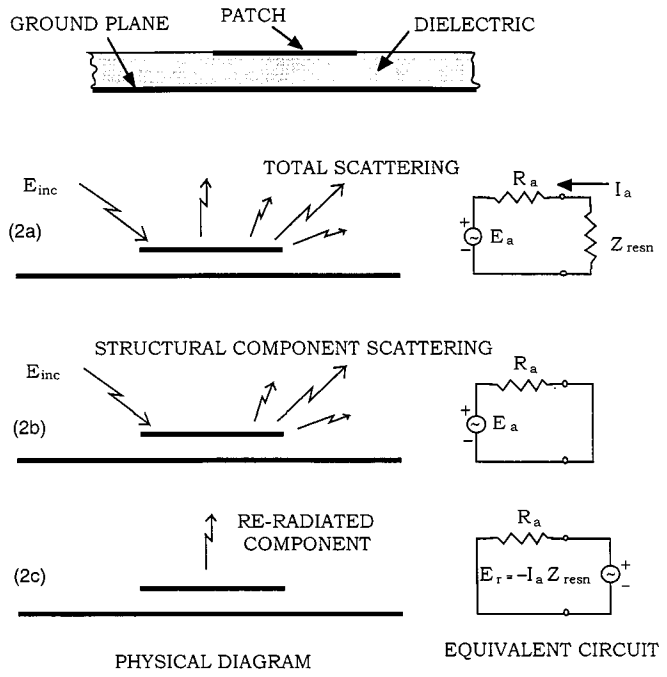

Fig. 2. Analysis of scattered field components using the compensation theorem.

these two separate circuits. We have tried to indicate the corresponding superposition of fields $\overline{E}_{\rm scatt} = \overline{E}'_{\rm scatt} + \overline{E}''_{\rm scatt}$ in the physical pictures. Since the generator E_a is present in the circuit Fig. 2(b), $\overline{E}_{\rm inc}$ is present in the corresponding physical picture and, consequently, so are all scattered fields *except the component due to the resonant fields interior of the patch resonator*. The resonator is (in this construction) short-circuited or detuned. These constitute the $\overline{E}'_{\rm scatt}$ component of the scattered field. It is plausible to assume that the fields scattered from the top conducting surface of patch differ negligibly from those which would be scattered from the portion of the ground plane immediately under the patch if the patch were removed. We therefore conclude that the component of scattered fields including those from the ground plane, diffraction from the edges of the large ground plane, mutual coupling between the auxiliary antennas, and reflections from the environment such as the walls of an (imperfect) anechoic chamber, is very nearly the same as would be scattered from the experimental setup if the patch was removed. Explicitly, we assume

$$\overline{E}'_{\rm scatt}\ \text{(antenna on ground plane with resonator short-circuited)} = \overline{E}_{\rm ref}\ \text{(no patch antenna on the ground plane).} \quad (1)$$

The generator E_a is absent from the equivalent circuit of Fig. 2(c). Correspondingly, the incident field is absent from the physical picture to the left of that circuit. The component of the scattered field in Fig. 2(c) $E''_{\rm scatt}$ is, therefore, due entirely to the resonant fields excited by E_r within the patch. The generator E_r excites the patch resonator radiation resistance just as a conventional input, giving rise to radiation with the same angular pattern as the field normally radiated by the patch antenna. This is, therefore, identified as the reradiated component of the scattered field

$$\overline{E}''_{\rm scatt} = \overline{E}_{\rm rerad}. \quad (2)$$

The radiated field of a patch antenna may be computed from equivalent magnetic currents that would need to circulate on the perimeter of the patch in order to confine the resonator fields [4]. From these magnetic currents the vector potential $\overline{F}$ and, finally, the fields can be calculated. In particular, the electric far-field phasor is obtained as $\overline{E}_{\rm re\text{-}rad} \sim -j\,k\,\overline{r}_o \times \overline{F}$. At the resonant frequency of the patch the resonator fields (therefore, the magnetic currents and the vector potential $\overline{F}$) are in phase with the incident field excitation. Taking the center of the patch on the ground plane as the reference point, the near-field components of the scattered field due to diffraction from the ground plane, etc., and the far-field reradiated components of scattered field are in phase quadrature. We assume that the frequency dependence of the patch resonator is well approximated by that of a simple tuned circuit. The addition of a feed introduces contributions from nonresonant modes into the equivalent circuit model [4]. Generally, these have only a minor effect on the unloaded Q parameter [5].

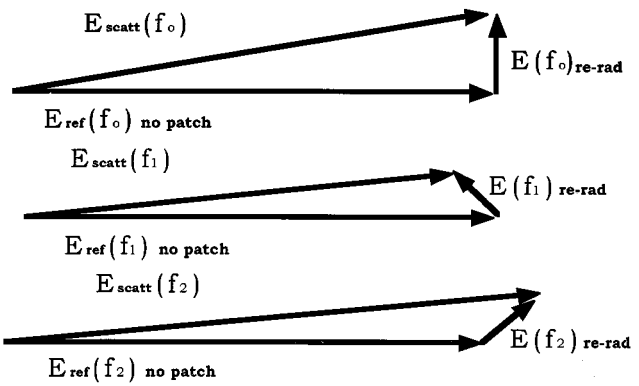

Fig. 3. Components of $\overline{E}_{\rm scatt}$ at resonance and at the half-power frequencies.

In accordance with the preceding analysis, the two components of the scattered field will combine at the receiving auxiliary horn #2 as illustrated in the phasor diagrams of Fig. 3. At the resonant frequency f_o, the reference component of scattered field is in phase quadrature with the reradiated component as shown in Fig. 3(a). At frequencies above and below the resonant frequency, say the half (reradiated) power frequencies, respectively, f_1 and f_2, the reradiated component of field is reduced in magnitude. More significantly, it is shifted in phase as shown in Figs. 3(b) and (c). Consequently, the magnitude of the total scattered field is, respectively, decreased or increased relative to the magnitude at resonance. For a simple resonance, it may be shown that the minimum magnitude of the total scattered field occurs at f_1 and maximum magnitude at f_2,

$$\frac{f_2 - f_1}{f_o} = \frac{1}{Q}. \quad (3)$$

The applicability of the above analysis and assumptions was tested in a series of experiments. Reference measurements of received power $|\overline{E}_{\rm ref}|^2$ versus frequency were taken with the complete experimental setup in the absence of any mounted patch antenna structure (1). The results are plotted in Fig. 4(a). The patch antenna structure was then mounted on the large ground plane, care being taken not to disturb the remainder of the setup in any way. Measurements of received power $|\overline{E}_{\rm scatt}|^2$ versus frequency were then repeated. Results for a typical structure are plotted in Fig. 4(b). The ratio of the powers (difference in dBm) at each data point (renormalized) is plotted in Fig. 4(c).

On the basis of the preceding analysis, we expect that at frequencies far off resonance (or when the resonant field within the patch is actually or theoretically suppressed) the patch antenna structure has a negligible effect. Consequently, in this (trivial) range, the field scattered by the patch on the ground plane is very much the same as the field scattered by the ground plane without the patch, cf. (1). The power ratio $|\overline{E}_{\rm scatt}|^2/|\overline{E}_{\rm ref}|^2$ is unity. Renormalization to the peak response is responsible for the shift of the corresponding decibel level in Fig. 4(c) from zero. To the first order, the same unity power ratio is found at the

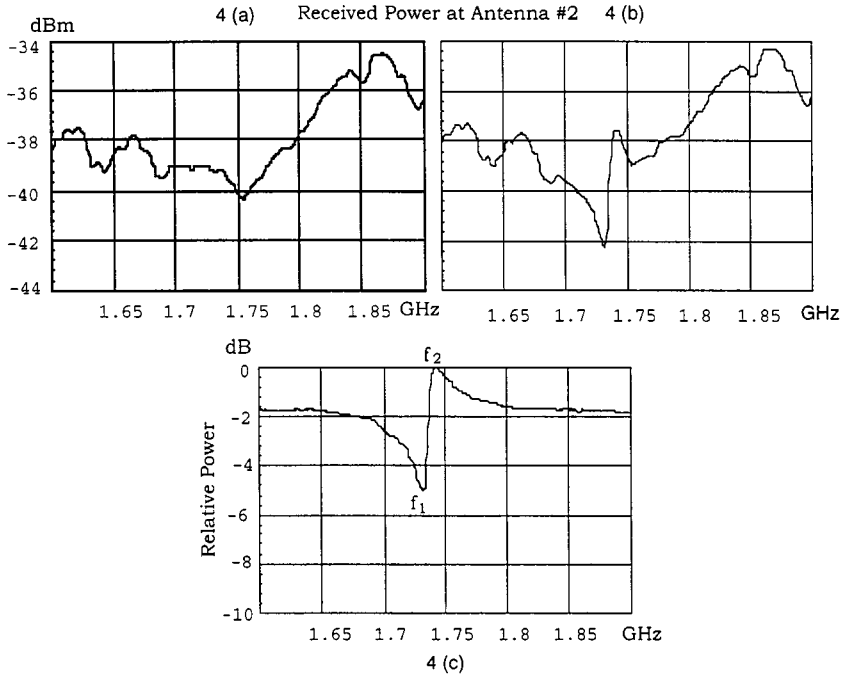

Fig. 4. Measurements of received power (decibels) versus frequency (gigahertz).

TABLE I
COMPARISON OF UNLOADED Q VALUES USING THREE DIFFERENT MEASUREMENT TECHNIQUES

dielectric const.	thickness (mils)	Q scattered	Q (S12)	Q smith chart
2.33	31	109	118	124
2.33	62	87	90	77
2.33	125	27	36	36
4.5	25	137	143	159
4.5	50	139	138	134
4.5	100	80	83	80
6	25	156	172	164
6	50	157	138	165
6	100	101	101	108
10.8	25	177	176	189
10.8	75	186	197	185

resonant frequency of the patch. This is due to the fact that the two components of scattered field $\overline{E}_{\rm rerad}$ (due to the patch) and $\overline{E}_{\rm ref}$ (scattered with no patch) are then in phase quadrature as explained in connection with Fig. 3(a). Note that vector subtraction of fields $|\overline{E}_{\rm scatt} - \overline{E}_{\rm ref}|$ would produce a contrary result, namely, a maximum difference at the resonant frequency, since the magnitude of $\overline{E}_{\rm rerad}$ is maximum at f_o.

Table I shows a comparison of values of the unloaded Q for a number of patch antenna structures calculated from scattering data Fig. 4(c) and that obtained by us on the patch resonators, as well as complete patch antennas fabricated from these structures by other techniques [5], [6]. Eleven antennas having the shape of a 90° annular sector (inner radius = 0.6 in, outer radius = 1.2 in) were tested. The dielectric constant and thickness of the substrate material are listed in the first two columns of the table. The column titled Q (scattered) lists values of unloaded Q obtained using the technique described in this paper. The column titled $Q(S_{12})$ presents values obtained from measurements of S_{12} (characterization of the cavity as a probe-excited transmission filter) using a network analyzer. A detailed description of the technique is contained in [6]. The column titled Q (Smith chart) presents values of the unloaded Q computed from measurements of S_{11} on complete patch antennas. This technique, which makes strong use of the Smith chart, is described in [5] and [6].

IV. CONCLUSION

A scattering method for measuring the unloaded Q of a prototype patch microstrip antenna resonator structure has been presented. It is seen that the form of measured data agrees with that predicted from our

assumptions and analysis. Further, values for the unloaded Q obtained by the scattering technique described in this paper are consistent with the values of the unloaded Q for patch resonator structures and for completed patch antennas fabricated from these structures obtained by other methods.

REFERENCES

[1] J. Aharoni, *Antennae*. Oxford, U.K.: Clarendon, 1946.

[2] J. D. Ryder, *Networks Lines and Fields*. New York: Prentice-Hall, 1949.

[3] W. K. Kahn, "Interrelation of radiation and scattering by antennas," in *Proc. NRSC' 94—11th Nat. Radio Sci. Conf.*, Cairo, Egypt, Mar. 1994, pp. 1, INV3–22, INV3.

[4] Y. T. Lo, D. Solomon, and W. F. Richards, "An improved theory for microstrip antennas with applications," *IEEE Trans. Antennas Propagat.*, vol. AP-29, no. 1, pp. 38–46, Jan. 1981.

[5] S. J. Weiss and W. K. Kahn, "Measurement of simple resonant equivalent circuits for microstrip antennas," *IEEE Trans. Microwave Theory Tech.*, vol. 44, pp. 1513–1516, Aug. 1996.

[6] S. J. Weiss, "A theoretical and experimental investigation of annular-sector microstrip antennas," Ph.D. dissertation, Dept. Elect. Eng. Comput. Sci., George Washington Univ., Washington, DC, May 1995.

Elimination of Impedance Anomalies in Single- and Dual-Polarized Endfire Tapered Slot Phased Arrays

Henrik Holter, Tan-Huat Chio, and Daniel H. Schaubert

***Abstract*—A method to eliminate bandwidth-limiting impedance anomalies or resonances in stripline-fed single- and dual-polarized tapered slot phased arrays is presented. For dual-polarized arrays, others have shown that the resonance with the lowest frequency is related to a cavity constituted by the dielectric region of the tapered slot element. Simulations have been performed to test if this cavity model also predicts the remaining resonances. It was found that the cavity model predicts some but not all of the resonances. However, it was found that all resonances in both single- and dual-polarized arrays have some dependence on the dielectric region. The resonances are effectively suppressed by introducing plated through vias in the element. The vias are positioned along the edges of the slotline, slotline cavity, stripline, and stripline stub. The analysis is performed with the finite-difference time-domain method by considering a unit cell in an infinite array.**

***Index Terms*—Dual-polarized antennas, phased-array antennas, slot antennas.**

I. INTRODUCTION

The tapered-slot element is a promising candidate for both single- and dual-polarized wide-band and wide-angle scanning phased arrays. A bandwidth in the order of $5:1$ over a scan volume of $\pm 45^{\circ}$ is achievable. Scan blindness and resonances limit the upper frequency band. The resonances seem to be especially serious for scanning in the H-plane. The purpose of this letter is to show a method to eliminate the resonances for both single- and dual-polarized tapered slot arrays. The tapered slot element is shown in Figs. 1 and 2. The element consists of a slotline and a slotline cavity etched in metal fins on each side of a dielectric. A stripline terminated in a stripline stub is located between the metal fins and feeds the element. The exponential opening of the slotline for the current element is determined by $R = 0.02\ \mathrm{mm}^{-1}$ [1]. A dual-polarized array can be designed by positioning the elements, as shown in Fig. 1. Metal walls must be positioned between the elements. If the metal walls are absent, that is the dielectric is continuos between the elements, several strong resonances will appear through the entire usable frequency band [2]. A single-polarized array can be formed if all the horizontal or vertical elements in Fig. 1 are removed. The metal walls between the elements are not needed for the single-polarized array. The analysis is performed with the finite-difference time-domain (FDTD) method by considering a unit cell in an infinite array [3], [4]. The element geometry requires a high resolution in FDTD. The FDTD cell size is 0.4 mm, which corresponds to 125–750 FDTD cells per free-space wavelength for the frequency range 1–6 GHz.

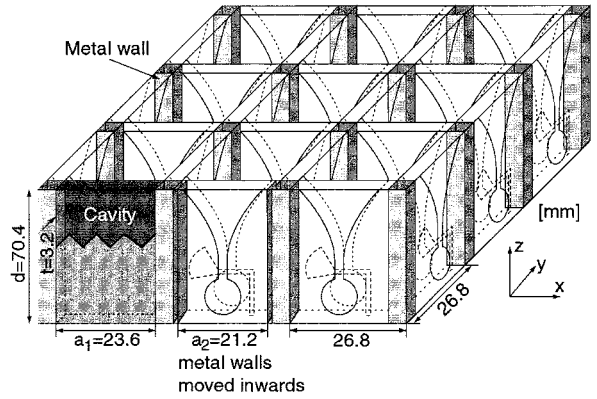

Fig. 1. A dual-polarized tapered slot array.

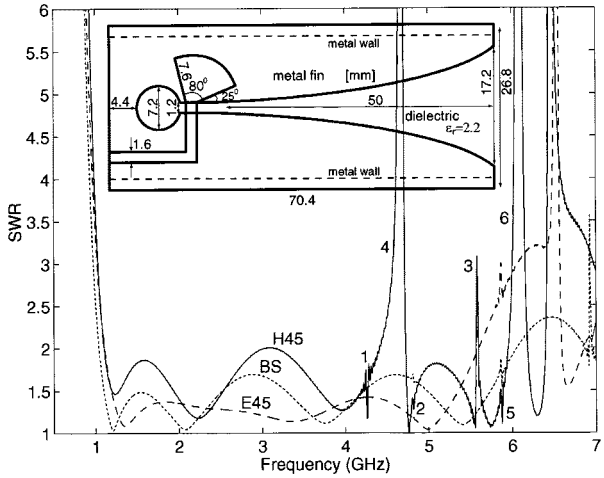

Fig. 2. Standing wave ratio (SWR) for the dual-polarized array. Broadside (BS), E-plane 45° (E45), and H-plane 45° (H45) scan. The first grating lobe appears at 6.56 GHz.

II. IDENTIFICATION OF THE RESONANCES

A model for the frequency of the first resonance in dual-polarized arrays has earlier been given in [5]. According to [5], the resonance is

Manuscript received April 13, 1999.

H. Holter is with the Department of Electromagnetic Theory, Royal Institute of Technology, SE-100 44 Stockholm, Sweden.

T.-H. Chio was with the University of Massachusetts, Amherst, MA 01003 USA. He is now with the DSO National Laboratories, Singapore, 118230 Republic of Singapore.

D. H. Schaubert is with the Department of Electrical and Computer Engineering, University of Massachusetts, Amherst, MA 01003 USA.

Publisher Item Identifier S 0018-926X(00)01285-0.

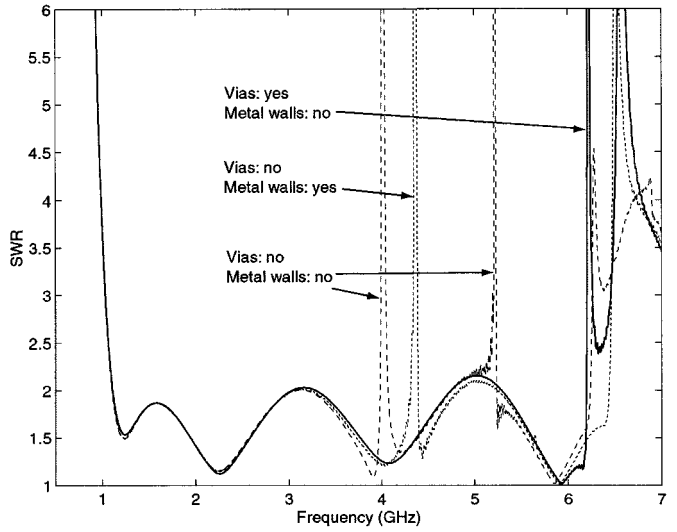

Fig. 3. SWR for the single-polarized array. H-plane 45° scan. The first grating lobe appears at 6.56 GHz.

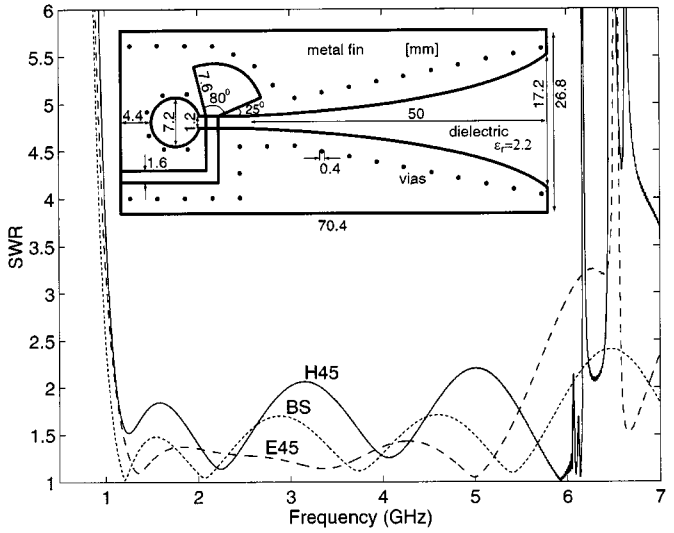

Fig. 4. SWR for the dual-polarized array. Broadside (BS), E-plane 45° (E45) and H-plane 45° (H45) scan. The first grating lobe appears at 6.56 GHz.

caused by the first resonance mode of a cavity constituted by the dielectric region as shown in Fig. 1. The cavity resonance frequency is approximately calculated by assuming that all walls but the front wall are perfect electric conductors. The open front wall is treated as a perfect magnetic conductor and the influence of the stripline and stripline stub is neglected.

Simulations were performed to examine if this cavity model can predict also resonances at higher frequencies in dual-polarized arrays. Fig. 2 shows the stripline standing wave ratio for broadside and 45° E- and H-plane scan. The first weak resonance at 4.26 GHz, marked "1" in Fig. 2, agrees well with the predicted 4.34 GHz first cavity resonance. The resonances marked "2" and "3" appear at 4.80 and 5.58 very close to the predicted 4.80 and 5.59 GHz cavity resonances. However, there are also resonances at 4.67, 5.84, and 6.09 GHz, marked "4," "5," and "6," which are not predicted by the cavity model. The resonances did not move after changing the scan angle to 30°, which shows that they are element phenomena not depending on the phasing of the array. To further test the cavity model and partially repeat the examination in [1] and [5], the metal walls where the orthogonal elements are overlapping were moved inwards 1.2 mm on each side as shown in Fig. 1. The cavity then becomes smaller, which should move the cavity resonances to higher frequencies. All resonances moved to higher frequencies, which show that they have some dependence on the cavity or dielectric region. Further, a single-polarized array, formed by removing all elements parallel to the x–z plane in Fig. 1, was simulated. The array was simulated both with and without metal walls between the elements. With metal walls there was a strong resonance at 4.36 GHz and a weak resonance at 5.65 GHz shown in Fig. 3. They can be related to the two first-cavity resonances at 4.34 and 5.59 GHz. Without the metal walls there were resonances at 4.02, 5.22, and 6.28 GHz. The resonances moved toward broadside when the scan angle was increased from 30 to 45°. Without the metal walls a TEM-mode as well as higher order modes can exist in the dielectric region. Since the dielectric region is loaded with striplines and stripline stubs and slotlines are also etched in the metal fins, it is difficult to predict what mode might exist and their resonance frequencies.

Nevertheless, the simulation results indicate that the resonances have some dependence on the dielectric region for both single- and dual-polarized arrays. No further investigations were performed to identify the resonances. Instead, methods to reduce or eliminate them were examined.

III. Elimination of the Resonances

All resonances moved to higher frequencies when the dielectric region was made smaller by moving the metal walls inwards for the dual-polarized array and by adding metal walls in the single-polarized array. This gives a clue to how to reduce the resonances. However, metal walls are impractical. Instead, vias were placed through the element and several different locations and number of vias were examined. Also, the metal walls between the elements in Fig. 1 were removed since they are inconvenient from a manufacturing point of view. The width of the vias was 0.4 × 0.4 mm (one FDTD cell). It was found that the via configuration shown in Fig. 4 eliminated all resonances below 6 GHz in both single- and dual-polarized arrays. The SWR for the dual-polarized array is shown in Fig. 4 and the SWR for 45° H-plane scan for the single-polarized array is shown in Fig. 3. The SWR for both the single- and dual-polarized arrays are almost exactly the same with vias in the elements. There is still a resonance at 6.18 GHz for the single- and dual-polarized array. There are about seven vias per dielectric wavelength at 6.0 GHz. With ten vias per wavelength, the small peaks visible at 6.06 GHz in Fig. 4 disappeared completely. With five vias per wavelength, there were narrow resonances at 5.7 GHz (SWR = 1.8) and 6.0 GHz (SWR = 2.7). When the vias around the slotline cavity were removed, there was a narrow resonance at 6.0 GHz (SWR = 2.7) and it remained (SWR = 2.6) with three vias around the cavity. More than six vias around the cavity did not improve the result. The cavity vias should not be positioned closer to the stripline-to-slotline transition than those shown in Fig. 4. As can be seen in Figs. 2 and 4, the broadside and the E-plane 45° scans are almost unaffected by the introduction of vias, which is expected from symmetry reasons.

IV. Summary and Conclusions

Impedance anomalies or resonances in single- and dual-polarized tapered slot phased arrays were eliminated by introduction of vias. The resonances are related to the dielectric region of the element. It is necessary to have at least seven vias per dielectric wavelength. Also, it is necessary to have vias around the slotline cavity. Since the slotline and stripline currents are concentrated close to the edges, it is possible to position the vias near those edges without too much interference.

REFERENCES

[1] T-H. Chio and D. H. Schaubert, "Parameter study and design of wide-band wide-scan dual-polarized tapered slot antenna arrays," IEEE Trans. Antennas Propagat., submitted for publication.

[2] D. H. Schaubert, "A gap-induced element resonance in single polarized arrays of notch antennas," in *IEEE Antennas Propagat. Symp. Dig.*, Seattle, WA, June 1994, pp. 1264–1267.

[3] H. Holter and H. Steyskal, "Broad-band FDTD analysis of infinite phased arrays using periodic boundary conditions," *Inst. Elect. Eng. Electron. Lett.*, vol. 35, no. 10, pp. 758–759, May 1999.

[4] ——, "Infinite phased array analysis using FDTD periodic boundary conditions-pulse scanning in oblique directions," *IEEE Trans. Antennas Propagat.*, vol. 47, pp. 1508–1514, Oct. 1999.

[5] G. J. Wunsch, "Radiation characteristics of dual-polarized notch antenna arrays," Ph.D. dissertation, Department of Electrical and Computer Engineering, Univ. Massachusetts, Feb. 1997.

Use of Minimum Phase Signals to Establish the Time Reference in Transient Radar Target Identification Schemes

Christoph Ohl, Edward J. Rothwell, Dennis Nyquist, and Kun-Mu Chen

***Abstract*—The minimum phase representation of the transient scattered-field response of aircraft targets is used to establish the time origin of a measured signal in reference to a stored target library. This allows time-shift-sensitive schemes such as the E-pulse method and neural networks to be used effectively. An example in which the wavelet spectra of unknown and library target responses are correlated demonstrates the viability of the technique.**

***Index Terms*—Electromagnetic transient scattering, synchronization.**

I. INTRODUCTION

Several ultrawide-band radar target identification schemes have recently been introduced, which use the early-time specular response at various aspects as the target feature set. The measured transient response of an unknown target is compared in some way with the stored responses of known targets and an identification decision is made. Comparison techniques may involve the use of direct correlation [1], neural networks [1], [2], E-pulse methods [3], or wavelet transforms [4].

An important difficulty that arises in implementing these schemes is that the time origin of the measured unknown target response is generally shifted with respect to that of the stored responses. This creates no difficulty in the case of direct correlation since the maximum value of the correlated waveform is used for identification. However, in the other comparison methods a small time shift between the measured and stored responses may introduce significant error [3], [5].

II. ESTABLISHING A SUITABLE TIME REFERENCE USING CEPSTRAL ANALYSIS

Simple techniques can be used to match the time references of the waveforms. The initial response can be located using an energy detector, but this is usually difficult under noisy conditions since the first reflection is often a low-amplitude specular reflection from the target nose or wingtip. Similarly, noisy conditions make it difficult to accurately locate and use the maximal target response as the reference.

Time-shifting problems are eliminated if just the magnitude of the frequency-domain response is considered (since a constant time shift only appears in the phase of the signal). However, since existing techniques employ comparison schemes directly in the time domain, it would be helpful if an algorithm could be employed that would remove the phase information from the time-domain signal. This can be accomplished using the minimum-phase representation (MPR) of the signal [6], [7].

Consider a measured radar signal represented as the sampled sequence $x(k)$, where k is the sampling index. The MPR of the signal is constructed using the algorithm

$$x_{\min}(k) = \mathrm{FFT}^{-1}\{e^{\mathrm{FFT}\{c(n)w(n)\}}\} \tag{1}$$

where

$$c(n) = \mathrm{FFT}^{-1}\{\ln\ \mathrm{FFT}\{x(k)\}\} \tag{2}$$

is called the "real cepstrum" of $x(k)$, and $w(n)$ is a windowing function given by

$$w(n) = \begin{cases} 2, & n > 0 \\ 1, & n = 0 \\ 0, & n < 0. \end{cases} \tag{3}$$

The MPR tends to $bunch$ the largest specular components near $t = 0$. Mathematically, if $\tilde{x}(k)$ is a waveform constructed using only the magnitude of the spectral response of $x(k)$, then

$$\sum_{k=0}^{m} |x_{\min}(k)|^2 \geq \sum_{k=0}^{m} |\tilde{x}(k)|^2 \tag{4}$$

for all m [6]. As an example, Fig. 1 shows the transient scattered-field response of a $1:72$ scale model SR-71 aircraft measured in the Michigan State University anechoic chamber transient scattering range [8]. The response was measured in the band 2–18 GHz at an aspect angle of 27.3° from nose-on incidence, with the incident field in the plane of the wings. The initial reflection from the nose is followed by reflections from the engines, wings, and vertical stabilizers. Fig. 2 shows the MPR of the measured SR-71 response constructed using (1). The largest reflections have been shifted to the origin, with the smaller reflections following.

The minimum phase signal provides an easily implemented time origin. All known target responses are stored in minimum-phase form and the minimum-phase representation of the unknown target response can be directly compared without worrying about unknown time shifts. However, since the phase information has been discarded, it is anticipated that the algorithms might lose some discrimination capacity.

III. CORRELATION OF WAVELET COEFFICIENTS

The discrete wavelet transform is a useful technique for storing radar data in an efficient manner. In [4], a technique was described wherein the stored data was reconstructed using the inverse wavelet transform and correlated with a measured signal for identification. An even more efficient method would be to correlate the wavelet spectrum of the measured signal with the spectra of the stored waveforms, thereby eliminating the time-consuming reconstruction step.

Manuscript received October 27, 1998; revised October 12, 1999.

The authors are with the Department of Electrical and Computer Engineering, Michigan State University, East Lansing, MI 48824 USA.

Publisher Item Identifier S 0018-926X(00)01286-2.

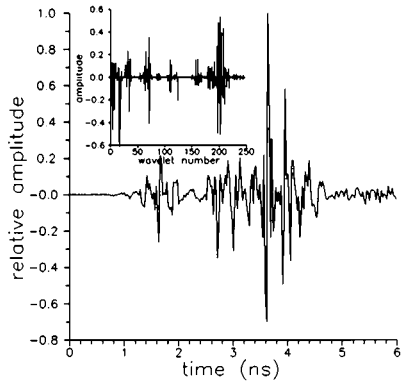

Fig. 1. Measured response of 1 : 72 scale model SR-71 aircraft at 27.3° incidence. Inset shows wavelet spectrum.

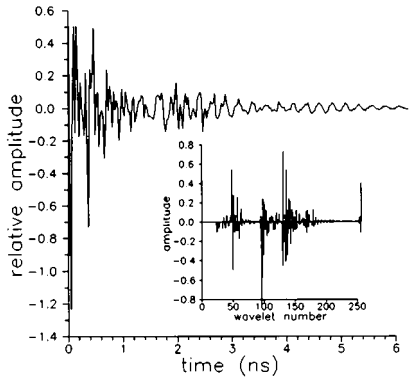

Fig. 2. Minimum-phase representation of measured response of 1 : 72 SR-71 aircraft model at 27.3° aspect angle. Inset shows wavelet spectrum.

Unfortunately, the wavelet spectrum is highly dependent on the time reference. However, if the minimum phase representations are used, there is no sensitivity to time shifts. Figs. 1 and 2 show the wavelet spectra of the measured and MPR responses of the SR-71 calculated using a 256-point Lemarie transform.

To demonstrate the use of this technique in target discrimination, the transient responses of two targets, the SR-71 and a 1 : 48 scale TR-1, were measured within the range of aspect angles 0–32° from nose-on. The MPR's of these signals were then created and the 32 largest components of the wavelet spectra of the minimum phase signals were stored in a data base. Then the response of the SR-71 at an aspect angle of 27.3° was chosen as the response of an unknown target. To identify this target, the wavelet spectrum of the MPR of the response was correlated with all wavelet spectra stored in the data base. Correlation was performed by multiplying the Fourier transforms of the wavelet spectra [found using the fast Fourier transform (FFT)], inverse Fourier transforming, and normalizing by the energy in the wavelet spectra. The maximal values of the resulting normalized correlation are shown in Fig. 3; identical wavelet spectra will produce a normalized correlation of unity. Since the correlation with the wavelet spectrum of the SR-71 at 27.3° is largest, the aircraft is correctly identified. In comparison, the maximum correlation with the wavelet spectra of the TR-1 is less than 0.6.

IV. Conclusions

The minimum phase representation provides a simple means for establishing the time reference of transient signals used in target identification. This allows techniques such as neural network storage and the early-time E-pulse method to be effectively employed. An example using correlation of the wavelet spectra has demonstrated the viability of the minimum-phase scheme.

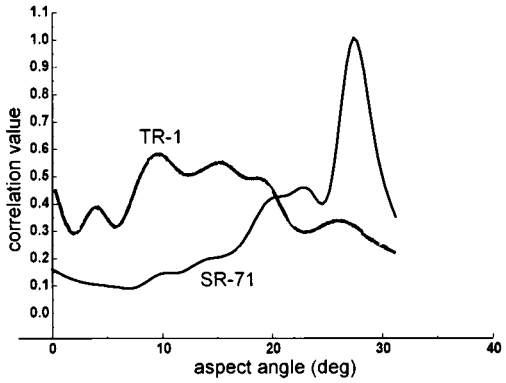

Fig. 3. Maximum values from correlating wavelet spectrum of 27.3° SR-71 minimum-phase target response with stored wavelet spectra of SR-71 and TR-1 minimum-phase target responses. Only largest 32 wavelet components used.

References

[1] H. J. Li and V. Chiou, "Aerospace target identification—Comparison between the matching score approach and the neural network approach," *J. Electromagn. Waves Applicat.*, vol. 7, no. 6, pp. 873–893, 1993.

[2] C. Y. Tsai, E. J. Rothwell, and K. M. Chen, "Target discrimination using neural networks with time domain or spectrum magnitude response," *J. Electromagn. Waves Applicat.*, vol. 10, no. 3, pp. 341–382, 1996.

[3] Q. Li, P. Ilavarasan, J. E. Ross, E. J. Rothwell, K. M. Chen, and D. P. Nyquist, "Combination of early-time and late-time based E pulses to improve target identification," *IEEE Trans. Antennas Propagat.*, vol. 46, pp. 1272–1278, Sept. 1998.

[4] E. J. Rothwell, K. M. Chen, D. P. Nyquist, J. E. Ross, and R. Bebermeyer, "A radar target discrimination scheme using the discrete wavelet transform for reduced data storage," *IEEE Trans. Antennas Propagat.*, vol. 42, pp. 1033–1037, July 1994.

[5] C. Ohl, "Target discrimination using the extinction-pulse technique and wavelet transforms combined with cepstral analysis," Master's thesis, Michigan State Univ., East Lansing, MI, 1997.

[6] A. V. Oppenheim and R. W. Schafer, *Digital Signal Processing*. Englewood Cliffs, NJ: Prentice-Hall, 1975.

[7] T. F. Quatieri and J. M. Tribolet, "Computation of the real cepstrum and minimum phase reconstruction," in *Programs for Digital Signal Processing*, New York: IEEE Press, 1979, pp. 7.2-1–7.2-6.

[8] E. Rothwell, K. M. Chen, D. Nyquist, J. Ross, and R. Bebermeyer, "Measurement and processing of scattered ultrawide-band/short-pulse signals," *Proc. SPIE Conf. Radar/Ladar Processing Applicat.*, vol. 2562, pp. 138–149, July 1995.

Circularly Polarized Circular Sector Dielectric Resonator Antenna

Matthew T. K. Tam and Ross D. Murch

***Abstract*—A circular sector dielectric resonator antenna (DRA) with circular polarization and a single feed is investigated and demonstrated. The design utilizes the radius to height ratio and feed position of the circular sector DRA to excite two resonant modes that are spatially orthogonal in polarization and in phase quadrature. Experimental results are provided for the design and these demonstrate that the circular sector DRA produces circular polarized radiation with axial ratio less than 3 dB over a 10% bandwidth.**

***Index Terms*—Circular polarization, circular sector, dielectric resonator antennas.**

I. Introduction

Recently, dielectric resonators have been demonstrated to be practical elements for antenna applications and have several merits including high radiation efficiency, flexible feed arrangement, simple geometry, and compactness [1]–[3]. In this letter, we investigate the possibility of producing circular polarization by utilizing circular sector dielectric resonator antenna (DRA) geometries that are formed by removing a sector (or equivalently a wedge) of dielectric material from a circular cylinder [4].

DRA's that exhibit circular polarization are not new. Circular and ring, DRA's using additional hardware comprising a 3-dB quadrature phase coupler or a 90° transmission-line phase shifter, have been reported [6], [7]. Rectangular DRA's fed by a single coaxial line or a slot, but without the use of any external quadrature phase devices, have also been investigated [8], [9]. In these rectangular DRA designs two degenerate modes that are spatially orthogonal are excited in phase quadrature and this approach is also widely adopted in microstrip patch designs [10]. In this letter, we report results of using this technique to achieve a single feed circularly polarized circular sector DRA. Potential advantages include compactness, simple construction, and 10% bandwidth with axial ratio (AR) less than 3 dB.

II. Theory

The geometry of a circular sector DRA is shown in Fig. 1, with sector angle β, radius a, and height d. The z-component electric field distribution of the $\mathrm{TM}_{\nu,\,p,\,m+\delta}$ mode inside the circular sector DRA can be written using the cavity model approximation [1], [4], as

$$E_z = A\,J_\nu\left(\frac{X_{\nu,p}}{a}r\right)\cos(\nu\phi)\,\cos\left[\frac{(2m+1)\pi}{2\,d}z\right] \qquad (1)$$

where A is an arbitrary constant and $\nu = 180^\circ/\beta$. The values $X_{\nu,\,p}$ are the roots of the characteristic equation $J'_\nu(X_{\nu,\,p}) = 0$ and the resonant frequency is given by

$$f_{\nu,\,p,\,m} = \frac{c}{2\pi\,a\sqrt{\epsilon_r}}\sqrt{X_{\nu,\,p}^2 + \left[\frac{(2m+1)\pi\,a}{2\,d}\right]^2}.$$

Manuscript received October 23, 1998; revised August 25, 1999. This work was supported by Hong Kong Research Grants Council.

The authors are with the Department of Electrical and Engineering, The Hong Kong University of Science and Technology, Clear Water Bay, Hong Kong.

Publisher Item Identifier S 0018-926X(00)01287-4.

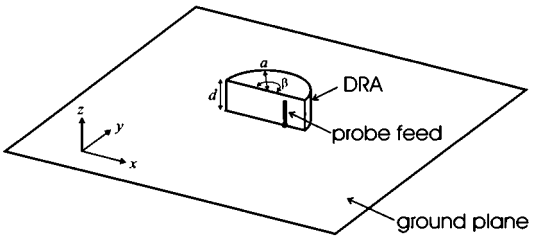

Fig. 1. Geometry of the circular sector DRA, $a = 18$ mm, $d = 15$ mm, $\beta = 180^\circ$.

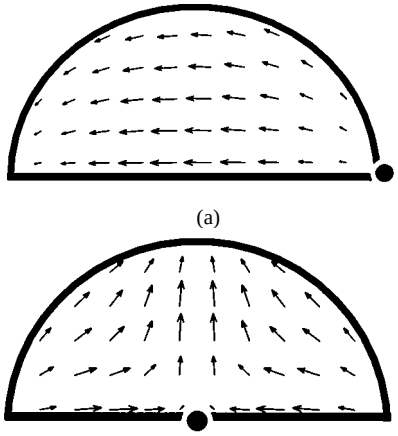

(a)

(b)

Fig. 2. Electric field distributions in a 180° sector DRA. Left: horizontally polarized $\mathrm{TM}_{1,\,1,\,\delta}$ mode. Right: vertically polarized $\mathrm{TM}_{2,\,1,\,\delta}$ mode.

To obtain circular polarized radiation from the sector DRA, two modes that have orthogonal polarizations and similar radiation patterns should be excited in quadrature phase. In our design, we utilize the fundamental resonant mode $\mathrm{TM}_{\nu,\,1,\,\delta}$ and the next lowest resonant mode $\mathrm{TM}_{2\nu,\,1,\,\delta}$ in a DRA with $\beta = 180^\circ$. In Fig. 2 electric field distributions for the $\mathrm{TM}_{1,\,1,\,\delta}$ mode (fed at right) and $\mathrm{TM}_{2,\,1,\,\delta}$ mode (fed at center) are shown in plane view using (1). Radiation from mode $\mathrm{TM}_{1,\,1,\,\delta}$ is polarized along the x–z plane while that from mode $\mathrm{TM}_{2,\,1,\,\delta}$ is polarized along the y–z plane. Sector DRA's with $90^\circ \le \beta \le 180^\circ$ show similar behavior.

To use these modes to produce circular polarization it is necessary to excite them in phase quadrature. A $+45^\circ$ phase shift can be obtained by driving the mode below its resonant frequency (or -45° by driving above its resonant frequency) until the magnitude of the reflection coefficient, $|S_{11}|$, is at -3 dB [8], [10]. Therefore, at a particular frequency, when the lower resonant mode is driven at -45° and the upper resonant mode is driven at $+45^\circ$, a total of 90° phase between the two modes can be obtained [10].

By letting the two resonant frequencies from the orthogonal modes be f_1 and f_2 with $f_1 < f_2$, the quadrature phase condition is fulfilled when

$$f_1 + \frac{\Delta f_1}{2} = f_2 - \frac{\Delta f_2}{2} \qquad (3)$$

where Δf is the 3-dB bandwidth of $|S_{11}|$. By choosing suitable values of a, d, ϵ_r and β such that (3) is satisfied (and the radiation intensity from the two modes are equal), a circular polarized DRA is achieved with low AR. Estimates of Δf for use in (3) can be obtained from measurements or calculations of the Q-factor.

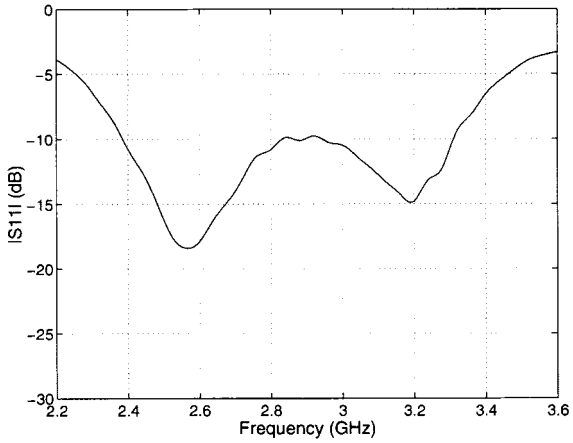

Fig. 3. Measurement of the reflection coefficient $|S_{11}|$ of the circularly polarized DRA.

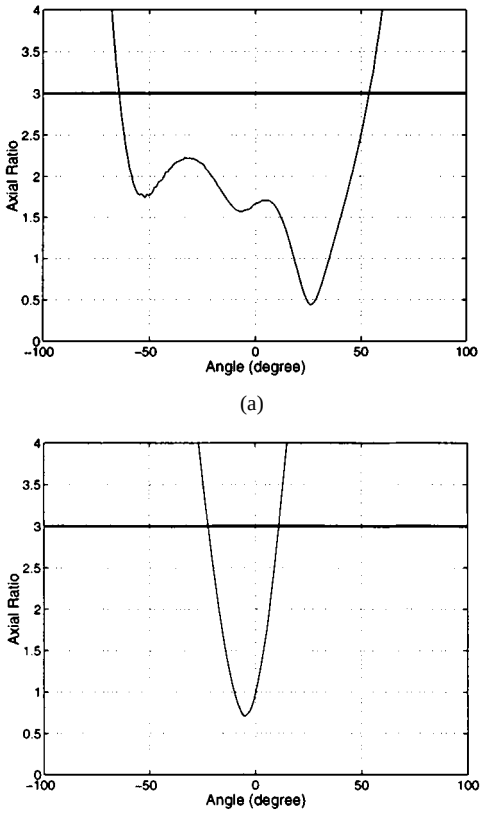

Fig. 4. Measurements of AR for the circularly polarized DRA at 2.71 GHz. (a) Horizontal x–z plane. (b) Vertical y–z plane (right).

III. Design Considerations

The beamwidth and bandwidth of the DRA with AR $<$ 3 dB depends on the geometry of the DRA. To provide wide bandwidth, the individual bandwidths of the two orthogonal polarizations must be wide so that the deviation from $\approx 90^\circ$ phase difference is small over a wide frequency range. Small values of ϵ_r and sector DRA's with open sector faces [4] are therefore chosen.

To ensure good beamwidth, the patterns of the two modes need to be as broad as possible. It is found that when $a/d > 1$, or when $\beta < 180^\circ$, the phase or amplitude variations of the patterns away from boresight become too large to achieve acceptable AR.

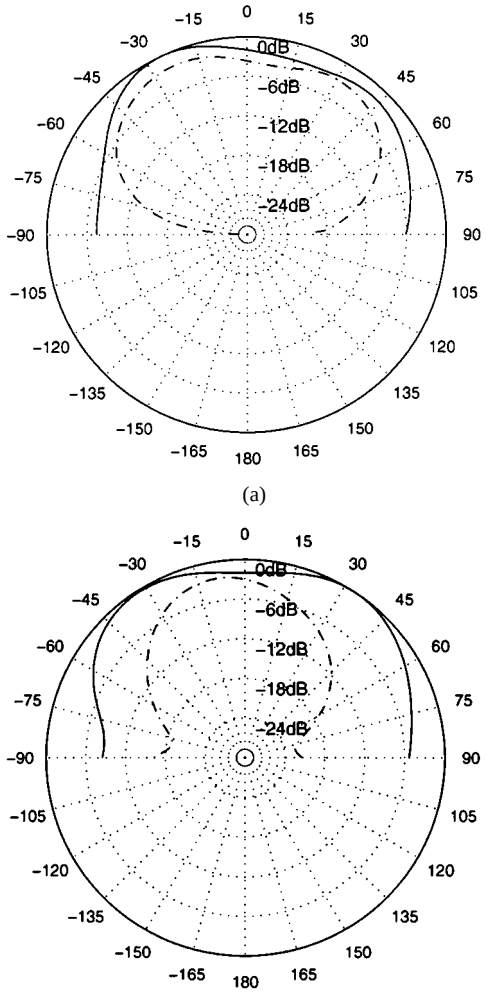

Fig. 5. Measurements of the antenna radiation patterns at 2.71 GHz. (a) Solid and broken lines are the major and minor axes of the polarization, respectively, in the horizontal x–z plane. (b) Vertical y–z plane.

From these observations, good circular polarization relies on the use of open face sector DRA's with low ϵ_r, β close to 180°, $a/d \approx 1$.

Impedance matching and excitation of both modes can be achieved by selecting an appropriate position for the feed along the radial edge between the DRA's center and outer edge. When fed from the center the $\mathrm{TM}_{2\nu,\,1,\,\delta}$ mode is primarily excited, while when fed from the edge, mode $\mathrm{TM}_{\nu,\,1,\,\delta}$ is primarily excited as in Fig. 2. Therefore, a position between the two extremes (on the sector face at radius around $a/2$) provides similar radiation patterns from both modes.

IV. Experimental Results

To demonstrate our design, the DRA, shown in Fig. 1, is built with $\beta = 180^\circ$, $a = 18$ mm, $d = 15$ mm, $\epsilon_r = 12$, and a ground plane of size 150 $\times$ 150 mm^2. The sector DRA is fabricated by machining "'ECCOSTOCK HiK" dielectric rod with $\epsilon_r = 12$ manufactured by Emerson and Cuming, Inc. Measurements are made using an HP8753D network analyzer in conjunction with an anechoic chamber in which a dual-polarized transmitting antenna is employed.

Fig. 3 plots the return loss $|S_{11}|$ of our DRA design and clearly shows the two resonances of the modes $\mathrm{TM}_{1,\,1,\,\delta}$ and $\mathrm{TM}_{2,\,1,\,\delta}$. At 2.71 GHz, the beamwidth with AR $<$ 3 dB, is 117° in the x–z plane and is 34° in the y–z plane as shown in Fig. 4. In Fig. 5, we illustrate the radiation

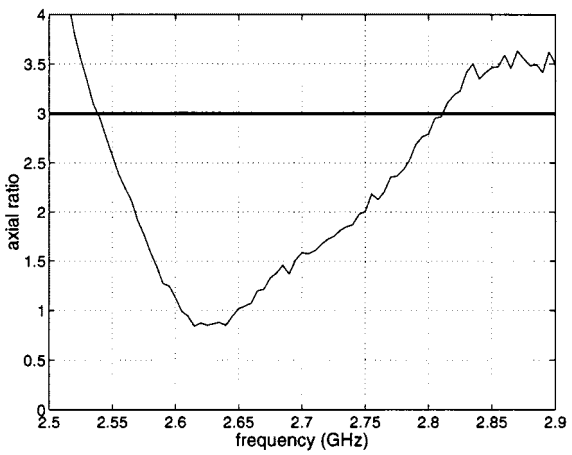

Fig. 6. Measurement of AR in the boresight direction versus frequency.

patterns by plotting the major and minor axes of the polarization ellipse for the x–z and y–z planes.

The AR bandwidth measurement is shown in Fig. 6 for the bore sight direction ($\theta = 0$, $\phi = 0$ in cylindrical coordinates) and is 2.54–2.81 GHz or 10% relative to the center frequency of 2.675 GHz. This wide bandwidth is thought to be due to the wide-band features of the sector DRA with open faces [4].

For size comparison, we compare our antenna (with volume 7.63 cm3), to the circularly polarized rectangular DRA described in [8]. After linear dimension scaling to the same dielectric material and resonant frequency as our design, the dimensions of the rectangular DRA become 23.27 × 21.08 × 23.27 mm^3 with volume 11.41 cm^3, which is 50% larger than our design. In terms of bandwidths our circular sector provides 10% ($\epsilon_r = 12$) while the rectangular DRA provides 6.6% ($\epsilon_r = 10.8$). In terms of beamwidth, however, the rectangular DRA is better with 110° in both planes

V. Conclusions

Techniques for producing circular polarization utilizing a single-feed circular sector DRA are described. Experimental results are provided for a particular circular sector DRA with $\beta = 180°$, $a = 18$ mm, $d = 15$ mm, and $\epsilon_r = 12$ operating at 2.71 GHz. The resulting volume of the DRA is 7.63 cm^3 and the 3-dB AR bandwidth is found to be 10% centered at 2.675 GHz. The beamwidth (axial ratio below 3 dB), measured at 2.71 GHz, is about 117° in the x–z plane and is 34° in the y–z plane. Advantages compared to other DRA designs include small size and wide bandwidth.

References

[1] S. A. Long, M. W. McAllister, and L. C. Shen, "The resonant cylindrical dielectric cavity antenna," *IEEE Trans. Antennas Propagat.*, vol. AP-31, pp. 406–412, Mar. 1983.

[2] R. K. Mongia and P. Bhartia, "Dielectric resonator antennas: A review and general design relations for resonant frequency and bandwidth," *Int. J. Microwave Millimeter-Wave Comput.-Aided Eng.*, vol. 4, no. 3, pp. 230–247, 1994.

[3] M. T. K. Tam and R. D. Murch, "Half volume dielectric resonator antenna designs," *Electron . Lett.*, vol. 33, no. 23, pp. 1914–1916 , 1997.

[4] ——, "Compact circular sector and annular sector dielectric resonator antennas," *IEEE Trans. Antennas Propagat.*, vol. 47, pp. 837–842, May 1999.

[5] H. Schrank, D. S. Dunn, and E. P. Augustin, "Measuring the gain of circularly or elliptically polarized antennas," *IEEE Antennas Propagat. Mag.*, vol. 36, pp. 49–51, Jan. 1994.

[6] R. K. Mongia, A. Ittipiboon, M. Cuhaci, and D. Roscoe, "Circular polarized dielectric resonator antenna," *Electron. Lett.*, vol. 30, no. 17, pp. 1361–1362, 1994.

[7] G. Drossos, Z. Wu, and L. E. Davis, "Circular polarized cylindrical dielectric resonator antenna," *Electron. Lett.*, vol. 32, no. 4, pp. 281–283, 1996.

[8] M. B. Oliver, Y. M. M. Antar, R. K. Mongia, and A. Ittipiboon, "Circularly polarized rectangular dielectric resonator antenna," *Electron. Lett.*, vol. 31, no. 6, pp. 418–419, 1995.

[9] BaltimoreK. P. Esselle, "Circularly polarized low-profile rectangular dielectric-resonator antenna: FD-TD and experimental results," in *1996 IEEE Antennas Propagat. Soc. Int. Symp.*, vol. 1, MD, 1996, pp. 577–580.

[10] D. M. Pozar and D. H. Schaubert, Eds., *Microstrip Antennas : The Analysis and Design of Microstrip Antennas and Arrays*. New York: IEEE Press, 1995.